Hindawi
Geofluids
Volume 2022, Article ID 6832272, 20 pages
https://doi.org/10.1155/2022/6832272

Research Article

Influencing Factors of Shale Permeability in the Longmaxi Formation, Southern Sichuan Basin and Northern Yunnan-Guizhou Depression

Changcheng Han,[1,2] **Geng Liu**,[1] **Cunfei Ma**,[3] **Ming Qi**,[1] **Yi Yang**,[1] **and Guan Li**[1]

[1]*College of Geology and Mining Engineering, Xinjiang University, Urumqi 830047, China*
[2]*Xinjiang Key Laboratory for Geodynamic Processes and Metallogenic Prognosis of the Central Asian Orogenic Belt, Urumqi 830047, China*
[3]*School of Geosciences, China University of Petroleum, Qingdao, 266580 Shandong, China*

Correspondence should be addressed to Geng Liu; liugeng729@foxmail.com

Received 9 May 2022; Accepted 25 June 2022; Published 22 July 2022

Academic Editor: Dengke Liu

The current paper studies the influencing factors of permeability in shales of the Longmaxi Formation, located in the southern Sichuan Basin, China. The methodologies used in the present study include overburden pore permeability experiments, whole rock analysis and geochemical tests, NMR measurements of fluid saturation, pore size distribution and specific surface area distribution, SEM and extraction of pore structure parameters, and core analysis. The results show the following: (1) high TOC and high maturity generate a large number of organic pores, which may improve the permeability of shale. (2) Mineral composition and rock relative permeability also have influence on permeability to a certain degree, since different minerals have different effects on shale permeability. Clay in the study area has an adverse effect on permeability. The results show that the organic-rich siliceous clay mixed shale facies in this area has the best permeability. (3) A large specific surface area and total pore volume are associated with good shale permeability, while average pore size does not correlate with permeability. A small fractal dimension of pore morphology and simple pore structure result in good permeability, and bedding is the key controlling factor for the anisotropy of shale permeability. (4) Water in shales can influence the permeability of microfractures by binding to clay minerals. Low permeability in shales with high bound water saturation suggests that water and clay mineral absorption may block flow channels, resulting in poor permeability. The purpose of this study is to clarify the influencing factors on shale permeability of the Longmaxi Formation in the study area and to provide a reference for the exploration and development of shale gas in this area of the Sichuan Basin.

1. Introduction

Shale gas refers to natural gas extracted from dark shale or organic-rich shale, self-generated and self-stored, which is accumulated in nanoscale pores, adsorbed on the surface of organic matter and clay minerals, and free in the micro-nanopores of organic matter shale [1–6]. Shale reservoirs are low porosity and low permeability and have a highly heterogeneous pore structure [7, 8]. As reflected by the US shale gas revolution in recent years, shale gas has become an important component of oil and gas production and a key point of increase in global oil and gas reserves [9–12]. China is rich in shale gas resources [13, 14]. The discovery of large shale gas fields and the establishment of three national shale gas demonstration areas mark a breakthrough in the exploration and development of shale gas in the Sichuan Basin [15], where the Wufeng and Longmaxi Formations are important exploration and development units [16–19]. The long-term productivity of shale gas wells is mainly controlled by the pore network and permeability of shale [20]. In previous studies, the permeability of shale is anisotropic [21]. Permeability is generally controlled by

shale mineral composition, porosity, pore connectivity, lithology, microfractures, TOC (total organic carbon), and maturity [22–26]. A combination of factors control shale permeability, and recent studies has attempted to shed light on these constraints. Recent studies indicate that fractures or water-blocking effects in the process of shale expansion have an impact on its permeability [27, 28]. Zhou and Zhao found that the fractal dimension of shale space correlates positively with shale permeability [29]. Tan et al. show that water saturation has a significant effect on gas-effective permeability [30]. However, the geochemical and geological characteristics of shales in other areas are different from those of marine shales in southern China, resulting in different petrophysical properties and fluid characteristics. There are few studies on the influencing factors of shale permeability in the Longmaxi Formation of the southern Sichuan Basin. This paper studies the influencing factors of gas shale permeability in the lower Silurian Longmaxi Formation. The influence of the geochemical and geological characteristics of shale on its permeability has been studied by using pressure attenuation and pulse attenuation methods. In addition, the influence of pore structure on permeability was analyzed by SEM. The purpose of this study is to clarify the influencing factors on the permeability of shale in the Longmaxi Formation of the southern Sichuan Basin and provide a reference for shale gas development in this research area.

2. Geological Setting and Experimental Samples

The main part of the study area is located in the southern part of the Sichuan Basin and the Yunnan-Guizhou North Depression, with the Longmaxi Formation as the target layer of this study (Figure 1). The thickness of the Longmaxi Formation is about 260 m, and its upper and lower boundaries are in contact with the Shiniulan and Wufeng Formations, respectively. This unit is mainly comprised of black carbonaceous shale and siliceous shale (Figure 2). The whole section is a high-quality shale gas reservoir with high TOC and good gas content. The shales of the Longmaxi Formation are thick and well preserved, making it a key unit for shale gas exploration. The samples were collected from the Longmaxi shale from 3 wells in the study area.

3. Experiments and Methodology

3.1. XRD Analysis. In this study, a RINT-TTR3 X-ray diffractometer was used to identify and analyze the mineralogical composition of shale samples from the study area. Twenty-four Longmaxi Formation shale samples from three wells were selected. Before the experiment, the samples were smashed to 200 mesh; mineral and clay powders were separated, dried, and tested. Mineral identification was achieved by obtaining the intensity of mineral signature peaks during X-ray diffraction.

3.2. Overpressure Measures Porosity and Permeability. These data of 48 shale samples from different wells were tested with a French Vinci Coreval 700 overburden porosimeter, to characterize the physical properties of the pores. The core column sample with a length of 3 cm was clamped by the holder and connected to the control center. Different wells adopt different overburden and confining pressures. In this experiment, an overburden pressure of 1.4 MPa and confining pressure of 7 MPa was used. Permeability measurements were done by the pressure pulse decay method, applying pressure to the core, and then measuring the pressure of the core to calculate permeability. Porosity measurements follow the principle of Boyle's law, which uses the expansion of helium to calculate porosity with the ideal gas equation according to pressure change and known volume.

3.3. NMR Experiment. Movable fluid saturation, bound water saturation, and porosity were measured in 20 samples of Longmaxi Formation shale using a low magnetic field NMR core analyzer (RecCore03). Fluid relaxation time in rock pores depends on the strength of the action of the solid surface on the fluid molecules [31]. If the action of the water molecules on the solid surface is strong, then the fluid is bound, and the bound fluid has a small T2 value; otherwise, the fluid would be movable. By observing the intensity and decay pattern of the hydrogen nucleus NMR signal and thus back calculating the fluid content in the pore space and the environment it is in, the lateral relaxation time T2 is derived from instrumental measurements, and the saturation is then determined from the shape and spread of T2 distribution.

3.4. Geochemical Analysis. The Leco carbon and sulfur tester were used in determining the TOC of the 56 shale samples. The carbon and sulfur in shale samples are heated for 2 h at high temperature (1000°C) under oxygen-rich conditions and oxidized to carbon dioxide and sulfur dioxide gases. The gases were processed in their corresponding absorber cells to absorb the corresponding infrared radiation, which was then forwarded by the detector as a signal, and the results were output by computer processing. In this study, only the TOC of the measured results was used. The maturity of the organic matter of 13 shale samples was measured using a J&M PMT IV spectrophotometer (by the Method for Determination of Reflectance of Specular Groups in Sedimentary Rocks, SY/T5124-1995). The spectrophotometer uses a light source that produces a wide range of wavelengths. A series of spectroscopic devices are used to produce a light source of a specific wavelength. After the light passes through the sample being measured, some of the light is absorbed. The carbon bitumen reflectance [24] was measured at an ambient temperature of 23 ± 3°C, relative humidity of <70%, a wavelength of 546 nm, a microscope magnification of 125x, a reflectance range of 0.1% to 10.0%, and a resolution of 0.01%. Carbon bitumen reflectance was then converted from $Ro' = 0.3364 + 0.6569 \times Rb$ to give the equivalent specular mass reflectance (Ro).

3.5. SEM Analysis. ZEISS scanning electron microscopy was used for pore structure and mineral analysis at the micron-nanometer scale. The samples were taken from L1 wells at various depths, cut into blocks of approximately 1 cc, and polished by argon-ion grinding to remove surface uneven parts and adhesions, and carbon-coated resin was mounted

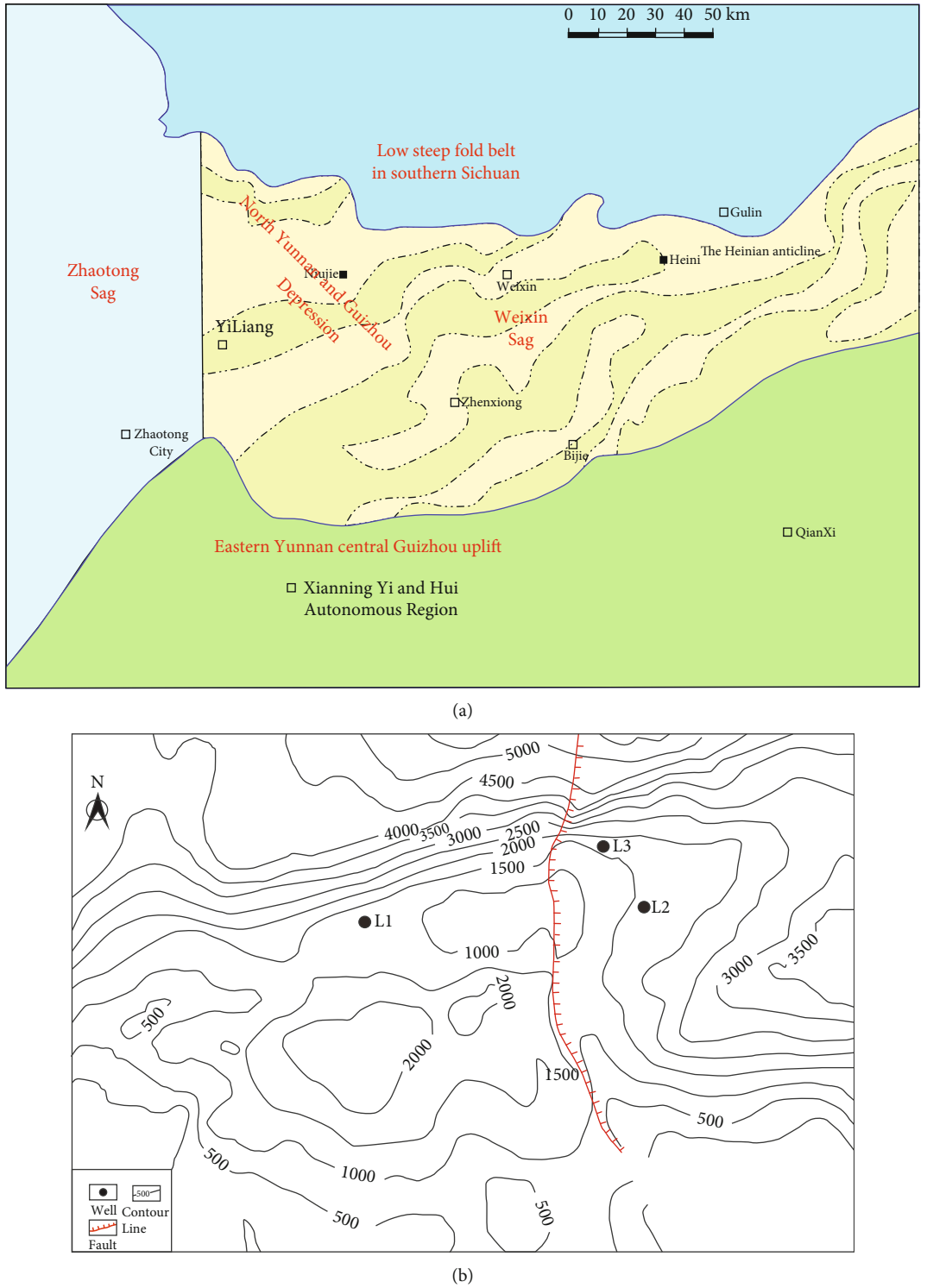

Figure 1: Maps showing the location of the study area. (a) Sketch map showing the Sichuan Basin and its adjacent area. (b) Map showing the well distribution, contour line, and faults of the study area.

to improve image quality for high-resolution imaging. Then, secondary electron (SE) and backscattered electron (BSE) images were obtained, and pore features were extracted using the software ImageJ, and the pore fractal dimension was calculated to investigate pore structure characteristics based on the images.

3.6. The Measurement of Pore Structure Parameters. The specific surface area, pore diameter, and total pore volume of 56 shale samples were measured by Micromeritics ASAP2420. This instrument uses helium and nitrogen gas as adsorbents. The following steps were carried out: 500 mg of shale sample was ground into a sieve (<60 mesh), then

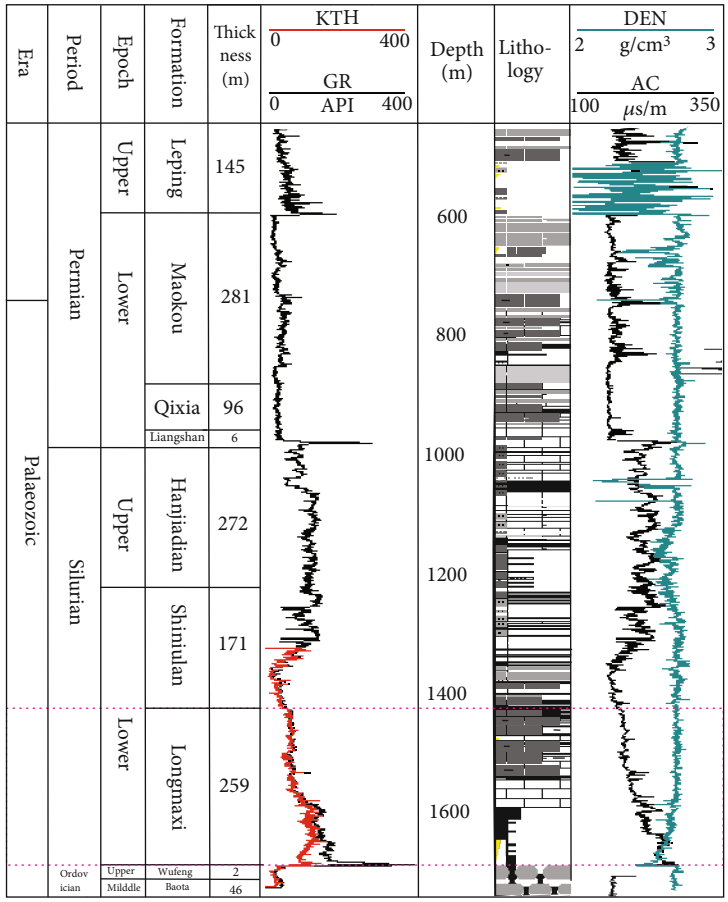

Figure 2: Lithofacies of a single well.

placed in a vacuum of 1×10^{-3} Pa for 3 h, and then heated at 120°C for 24 h to remove adsorbed moisture and volatiles, before testing. The pore size and specific surface area are obtained using the surface analysis system. The specific surface area measured ranges from 0.0005 to 5000 m^2/g, pore volume is <0.0001 cc/g, and pore size ranges from 0.35 to about 500 nm.

4. Results

4.1. Organic Geochemical Characteristics. Experimental results in this study comprise data from 23 samples from 3 different wells. Our results show that TOC values of Longmaxi Formation shale range from 1.1 to 4.9%, with values mainly between 2% and 3%, and an average TOC value of 2.9% (Figure 3). The measurements show that the TOC value increases with depth (Table 1). The types of organic matter present mainly type II (mostly type II_1 with some type II_2), and the type of organic matter is good. Organic matter maturity can reflect the hydrocarbon generation capacity of shale. In our samples, organic matter maturity is 2.11%-2.71%, with an average of 2.38%. This means they are in the overmature stage and generate dry gas. In general, the organic matter content is high and has good hydrocarbon generation potential.

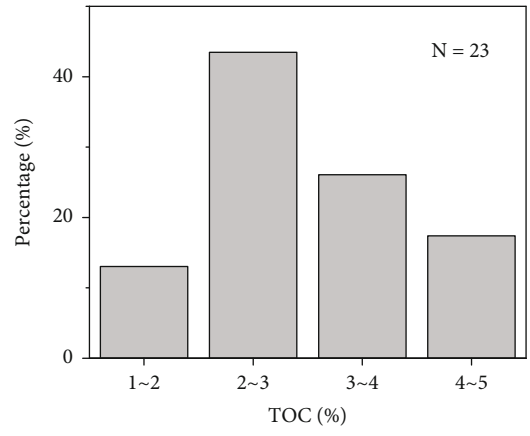

Figure 3: Histogram of TOC content distribution in Longmaxi Formation shale of the study area.

4.2. Mineral and Lithofacies Characteristics

4.2.1. Mineral Composition. The results of whole rock and clay analyses from 24 samples from three wells were selected for this study. The results from Figure 4 show that the minerals in this area consist mainly of quartz, feldspar, carbonate minerals, clay minerals, and a small amount of pyrite.

Table 1: TOC, organic matter type, and Ro of some Longmaxi Formation shales in the study area.

Sample number	Depth (m)	TOC (%)	Ro (%)	Organic matter type	Sample number	Depth (m)	TOC (%)	Ro (%)	Organic matter type
L1-1	1027.0	1.10			L2-3	1659.9	2.00		
L1-7	1039.5	1.10	2.15	II_2	L2-5	1665.7	2.40	2.51	
L1-14	1057.9	2.60			L2-7	1668.8	2.40		
L1-17	1063.1	2.70	2.11	II_2	L3-3	1479.3	2.57	2.20	II_1
L1-20	1069.4	3.10			L3-5	1483.3	2.37	2.23	
L1-23	1075.3	3.50	2.24	II_2	L3-8	1489.5	3.35	2.26	II_1
L2-1	1654.4	1.90	2.47		L3-11	1498.6	4.28	2.54	II_1

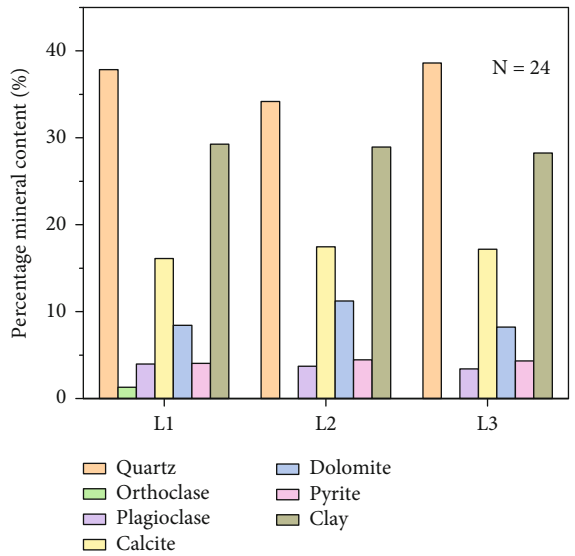

Figure 4: Histogram of mineral content distribution in the studied wells of Longmaxi Formation shale.

The percentage quartz content ranges from 28.1% to 45.7%, with an average of 36.3%; feldspar ranges from 1.1% to 10.7%, with an average of 3.9%; carbonate minerals range from 14.6% to 47.8%, with an average of 26.6%; a small amount of pyrite is also present, ranging from 2.7% to 6.3%, with an average of 4.3%; clay minerals range from 18.2% to 37.9%, with an average of 28.9%. The clay mineral content ranges from 18.2% to 37.9%, with an average of 28.9%. The clay mineral content is dominated by illite/smectite formation and illite, with an average percentage content of 47.2% and 36.3%, respectively, followed by chlorite with a percentage content of 16.5%. The longitudinal distribution of mineral content (Figures 5 and 6) shows that the clay mineral content of the study area decreases with depth and the brittle mineral content increases with depth.

4.2.2. Lithofacies Characteristics. A total of 30 Longmaxi shale samples from 3 wells were selected for whole rock analysis and subsequent lithofacies classification (Figure 7). The lithofacies present in the study area are mainly mixed shale, comprising organic matter-rich and organic matter-poor shales with 2% TOC according to the previous studies [32]. The samples from well L1 mainly developed organic-poor siliceous clayey mixed shale facies, organic-rich siliceous clayey mixed shale facies, organic-rich mixed shale facies, and organic-rich siliceous-calcareous mixed shale facies. The samples from well L2 mainly developed organic-rich mixed shale facies, as well as organic-rich siliceous-calcareous mixed shale facies. The samples from well L3 are made up of organic-rich siliceous clayey mixed shale facies with a small amount of organic-rich mixed shale facies and organic-rich siliceous-calcareous mixed shale facies (Table 2).

(1) Mixed shale facies (M): average contents of siliceous minerals, carbonate minerals, clay minerals, and TOC in the study area are 38.06%, 29.5%, 28.07%, and 3.09%, respectively

(2) Siliceous clay mixed shale facies (M-2): this is the most developed lithofacies in the study area, with an average siliceous mineral content of 42.88%, carbonate mineral content of 21.55%, clay mineral content of 31%, and TOC of 2.49%

(3) Siliceous-calcareous mixed shale facies (M-1): average contents of siliceous, carbonate, and clay minerals, as well as TOC, are 37.27%, 36.9%, 21.83%, and 4.33%, respectively

(4) Clay-bearing siliceous shale phase (S-3): the siliceous minerals in this phase averaged 49.8%, carbonate minerals averaged 14.85%, clay minerals averaged 30.15%, and TOC averaged 2.51%

4.3. Shale Pore Characteristics

4.3.1. Pore Types. The analysis of SEM photographs obtained shows that the Longmaxi Formation shale samples collected mainly developed organic pores, microfractures, intergranular pores, and intragranular pores, apart from other pore types.

(1) Organic pores: pores produced during hydrocarbon generation through the transformation of organic matter are defined as organic pores, which are generally irregular, vesicular, or elliptical. Organic pores are generally a few nanometers in size and are interconnected to some extent (Figure 8(a)). Organic pores are important storage spaces for shale, with

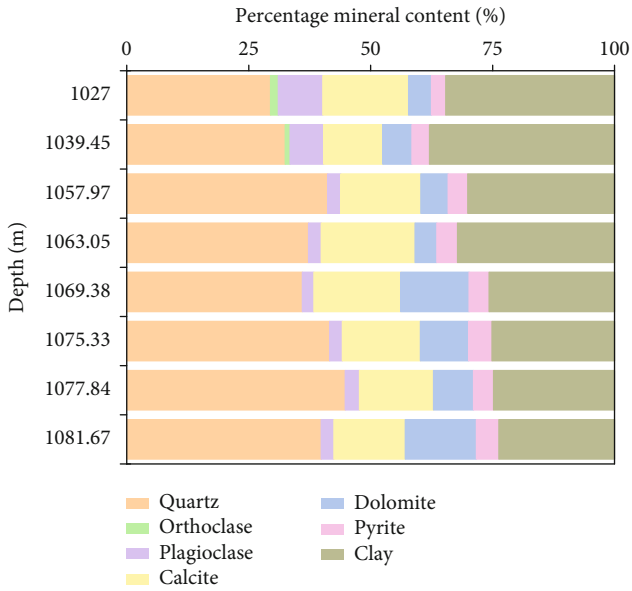

Figure 5: Vertical distribution map of mineral content of in well L1 (Longmaxi Formation).

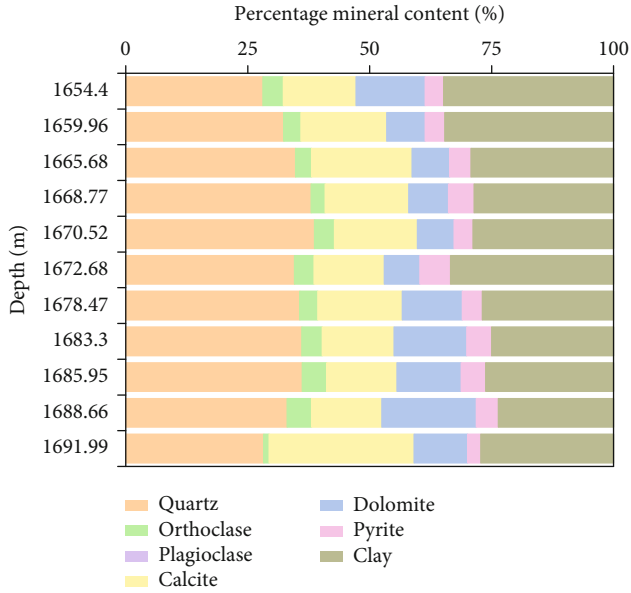

Figure 6: Vertical distribution map of mineral content in well L2 (Longmaxi Formation).

the potential for increasing the specific surface area of the whole shale pore system, thus increasing gas adsorption. It is worth noting that an organic matter-rich network of interconnected pores can improve gas permeability [33]

(2) Microfractures: microfractures (Figure 8(b)) are produced by the rupture of shale under stress and are the main seepage channel and storage space for free gas in shale reservoirs. While other types of pores are interconnected, microfractures are generally open, which is not only conducive to shale gas enrichment but also makes them the main channel for shale gas seepage and migration [34]

(3) Intercrystalline pores: these pores mainly occur in the interior of raspberry-like pyrite aggregates (Figure 8(c)), which are relatively common in shale. They are formed without close packing during crystal growth and are interconnected to a certain degree

(4) Intragranular pores: these pores mainly occur on the surfaces of carbonate minerals and quartz (Figure 8(d)). Due to the differences in the physical and chemical properties of different minerals, intragranular pores with different genetic mechanisms are formed, and mineral dissolution is common. Intragranular pores can provide large spaces for gas storage, and when dissolution is strong, connectivity between organic pores and intergranular pores increases, forming gas percolation channels

(5) Intergranular pores: these pores develop on the interface between brittle mineral particles or are supported by the latter (Figures 6(e) and 6(f)). Intergranular pores generally have good connectivity and can improve good gas seepage channels

4.3.2. Pore Physical Characteristics. Three types of permeability parameters were obtained from the experimental analysis of the overburden permeability of 36 shale samples from three wells in the study area. Firstly, the overburden permeability of 13 samples from the vertical laminae (Figure 9) was mainly distributed in two intervals of 0.0001 mD~0.001 mD and 0.001 mD~0.01 mD; these samples did not contain microfractures and showed extremely low permeability. The data obtained from both experimental porosity determination methods show a weak positive correlation with permeability (Figure 10), indicating that increasing porosity affects increasing permeability and that vertical permeability can be approximated to the matrix permeability. Secondly, the overburden permeability measured for 12 samples with parallel lamination (Figure 11) is predominantly distributed in the 0.01 mD to 0.1 mD interval, with a small number of samples distributed in the 0.1 mD to 1 mD range. The permeability of horizontal laminae is one order of magnitude higher than that of vertical laminae. Finally, the permeability of the eight samples with microfractures (Figure 12) has a wide range of distribution from 0.01 to 100 but is mainly concentrated between 1 mD and 10 mD, which is very high compared to the permeability of vertical laminae, showing the extent to which microfractures affect the permeability of shale.

4.3.3. Pore Structure Characteristics. The following data were obtained through low temperature nitrogen adsorption experiments on 22 shale samples from 3 wells (Table 3). Pores were classified into three pore types according to the IUPAC pore diameter classification method: macroporous (≧50 nm), mesoporous (2~50 nm),

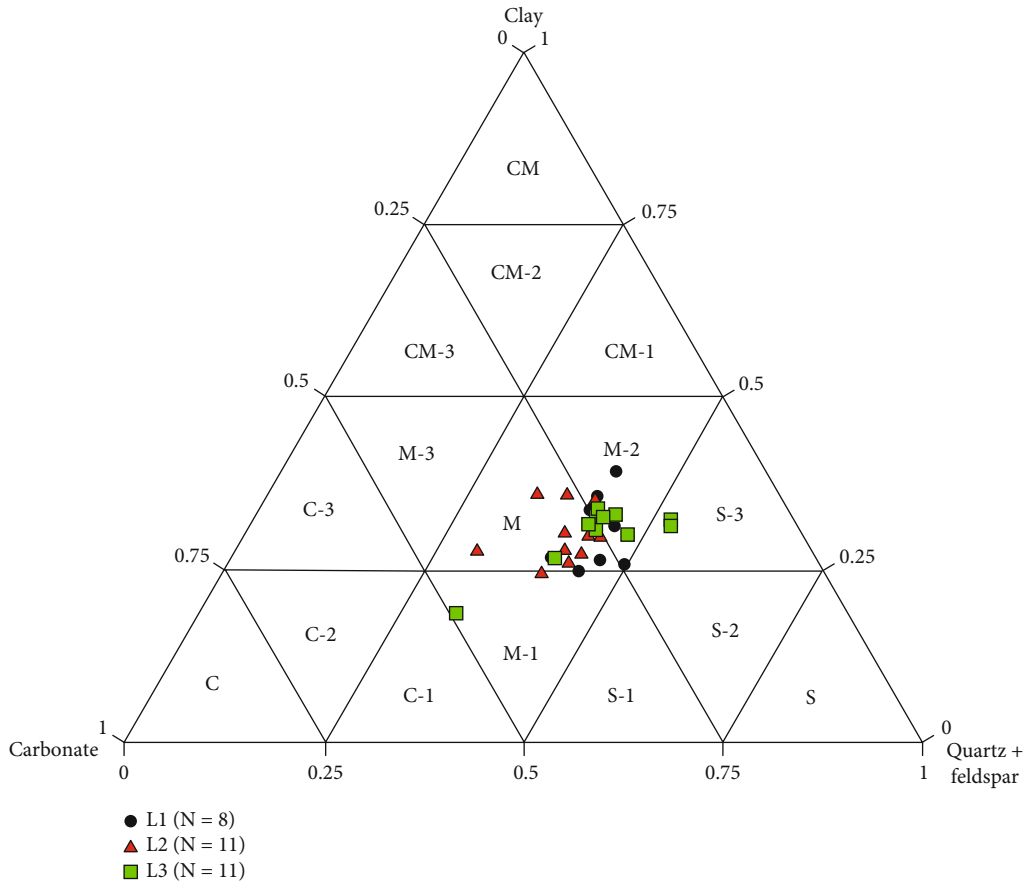

Figure 7: Ternary diagram showing lithofacies classification. (a) Siliceous rock facies combination (S). S: siliceous shale facies; S-1: siliceous-calcareous shale facies; S-2: calcareous clay-bearing siliceous shale; S-3: clay-bearing siliceous shale facies. (b) Lime shale facies combination (C). C: lime shale facies; C-1: siliceous lime shale facies; C-2: siliceous clay lime shale facies; C-3: clay-bearing calcareous shale facies. (c) Clay shale facies combination (CM). CM: clay shale facies; CM-1: silica-bearing clay shale facies; CM-2: lime-bearing siliceous clay shale facies; CM-3: lime-bearing clay shale facies. (d) Mixed shale facies combination (M). M: mixed shale facies; M-1: silica-bearing lime mixed shale facies; M-2: clay mixed shale facies; M-3: lime-bearing clay mixed shale facies.

Table 2: Mineral composition and lithofacies classification of the Longmaxi Formation in the study area.

Sample number	Quartz	Feldspar	Calcite	Dolomite	Pyrite	Clay	Clay mineral composition				TOC	Lithofacies
							I/S	It	C	I/S		
L1-1	29.5	10.7	17.6	4.7	2.9	34.6	45	40	15	10	1.1	Organic-poor organic matter-bearing siliceous clay mixed shale facies
L1-7	32.5	7.9	12.1	6	3.6	37.9	42	41	17	10	1.1	Organic-poor organic matter-bearing siliceous clay mixed shale facies
L2-1	28.1	4.2	14.9	14.2	3.8	34.8	51	29	20	5	1.9	Organic-poor mixed shale facies
L2-3	32.4	3.5	17.6	7.9	4	34.6	42	33	25	5	2.0	Organic-rich mixed shale facies
L2-5	34.8	3.3	20.6	7.7	4.4	29.2	41	34	25	5	2.4	Organic-rich mixed shale facies
L3-2	35.8	4.8	18.8	3.9	4.3	32.4	39	36	25	10	2.3	Organic-rich siliceous clay mixed shale facies
L3-3	40.3	2.7	17.0	4	4.4	31.6	38	38	24	10	2.6	Organic-rich siliceous clay mixed shale facies
L3-5	45.7	3.6	11.6	3	5.8	30.3	43	38	19	10	2.4	Organic-rich siliceous clay mixed shale facies

Note: C: chlorite; I: illite; S: smectite; I/S: illite/smectite formation.

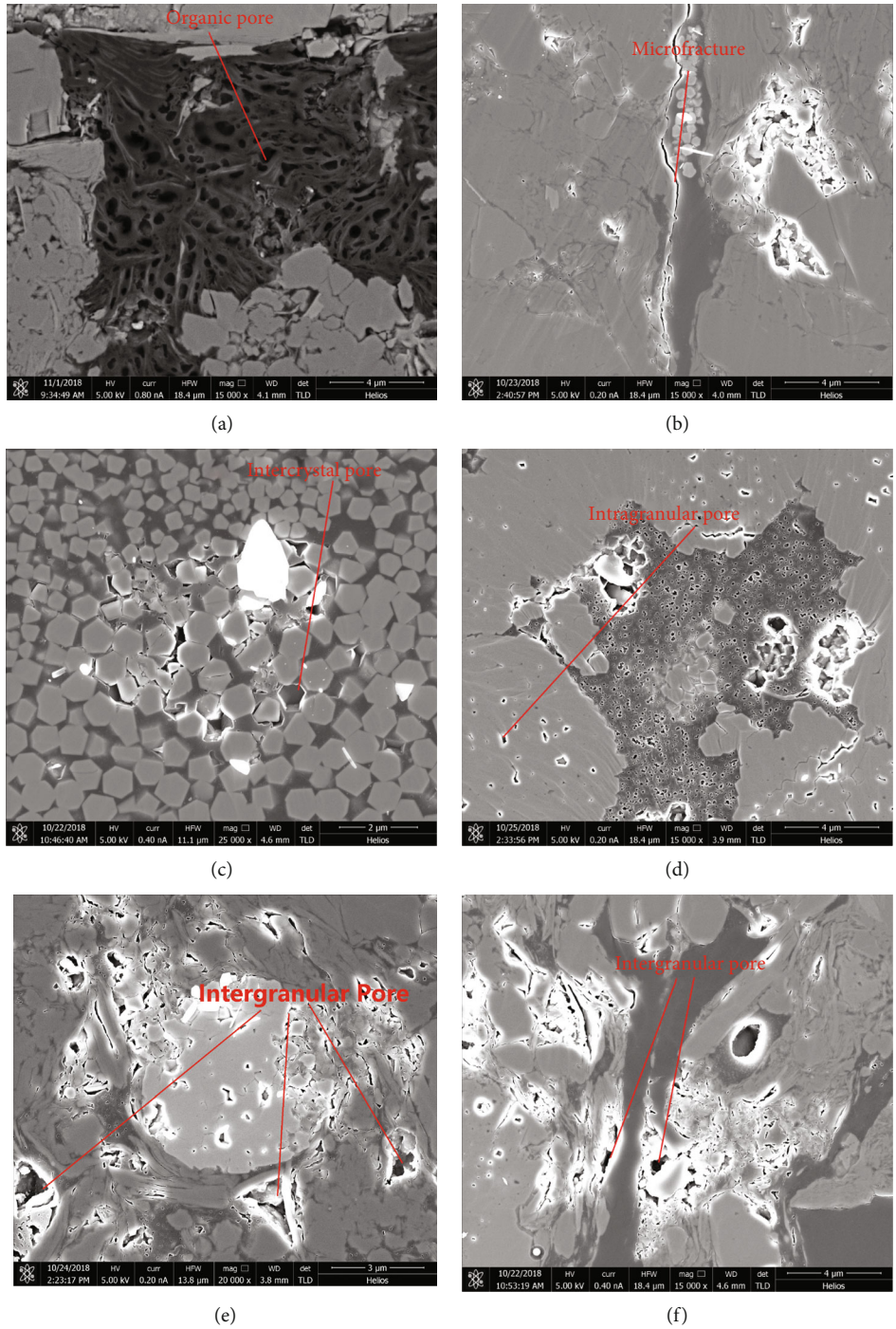

Figure 8: Pore types in Longmaxi Formation shales. (a) Well L1, organic pore, Longmaxi Formation, 1057.97 m. (b) Well L1, microfracture, Longmaxi Formation, 1069.38 m. (c) Well L1, intergranular pore, Longmaxi Formation, 1081.67 m. (d) Well L1, intragranular pores, Longmaxi Formation, 1063.05 m. (e) Well L1, intergranular pore, Longmaxi Formation, 1075.33 m. (f) Well L1, intergranular pore, Longmaxi Formation, 1081.67 m.

and microporous (≦2 nm). The average pore diameters of the shales in the study area range from 2.20 to 10.40 nm, with an average of 8.93 nm, all of which are in the mesoporous range. The BET-specific surface area ranges from 16.20 to 31.70 m^2/g, with an average of 23.18 m^2/g, and the specific surface area of each well increases with depth (Table 3). BJH Vtotal values range from 0.025 to 0.036 cm^3/g with a mean value of 0.032 cm^3/g, again increasing with depth. Overall, the pores of mud shale reservoirs in the study area have a large specific surface area and are good shale gas reservoirs.

Pore extraction was carried out using the software ImageJ on the Longmaxi Formation shale samples from well

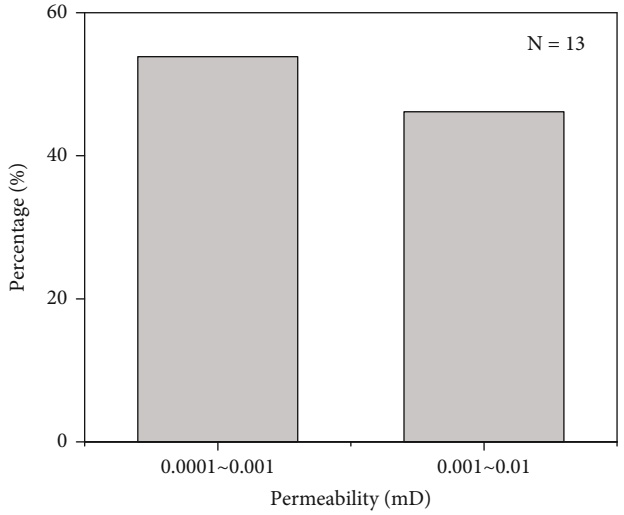

Figure 9: Permeability distribution histogram of vertical bedding.

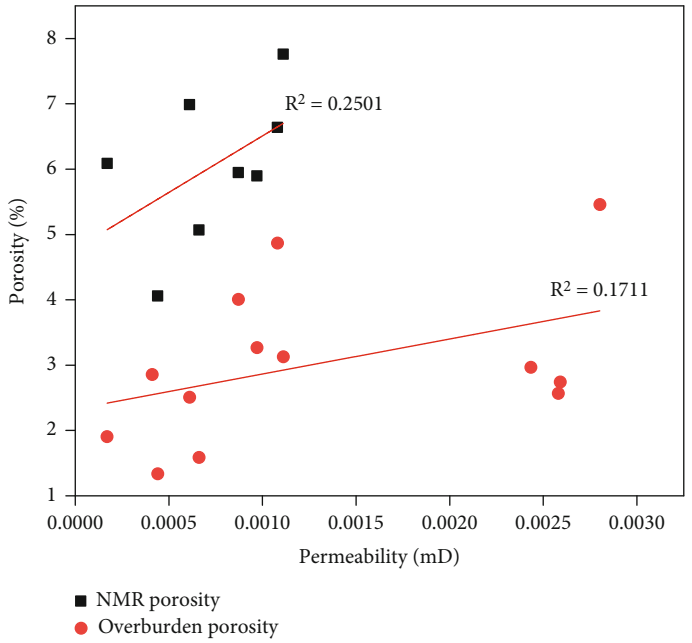

Figure 10: Pore permeability diagram.

L1 (Figure 13), followed by data processing to calculate pore fractal dimension (Figure 14). The results are shown in Table 4. According to fractal theory, the larger the fractal dimension, the more complex the pore morphology will be [35]. As shown in Figure 13, the fractal dimension of L1-14 is the smallest, indicating that its pore morphology is relatively simple compared to L1-20 and L1-24, while the fractal dimension of L1-20 pores is the largest, indicating a complex pore morphology.

4.4. Bedding Features. The shale of the Wufeng-Longmaxi Formation and its periphery mainly shows two kinds of bedding: horizontal bedding and massive bedding, with bedding and nonbedding fractures [36–39]. Likewise, horizontal and massive bedding are also prevalent in the study area.

(1) Horizontal bedding: it is generally believed that this kind of bedding is formed by the precipitation of substances from suspended solids or solutions under relatively stable hydrodynamic conditions [38]. Horizontal bedding (Figures 15(a)–15(b)) is widespread in Longmaxi Formation shale, which indicates slow deposition in a quiet water environment

(2) Massive bedding: the shale section presenting block bedding (Figures 15(c)–15(e)) contains many graptolite fossils, which indicates that the deposition rate

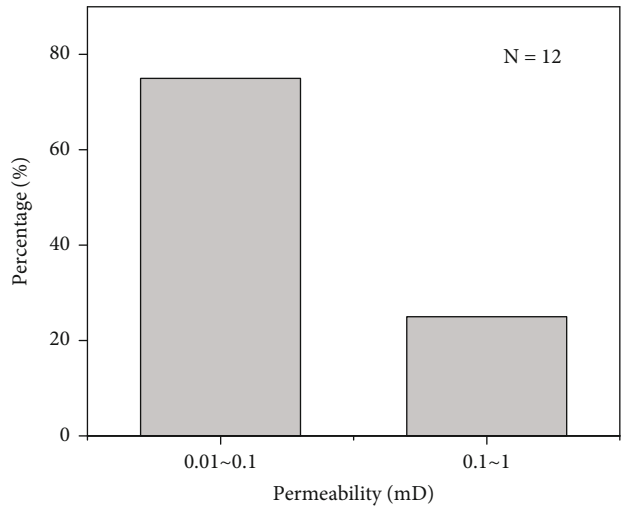

Figure 11: Permeability distribution histogram for parallel bedding.

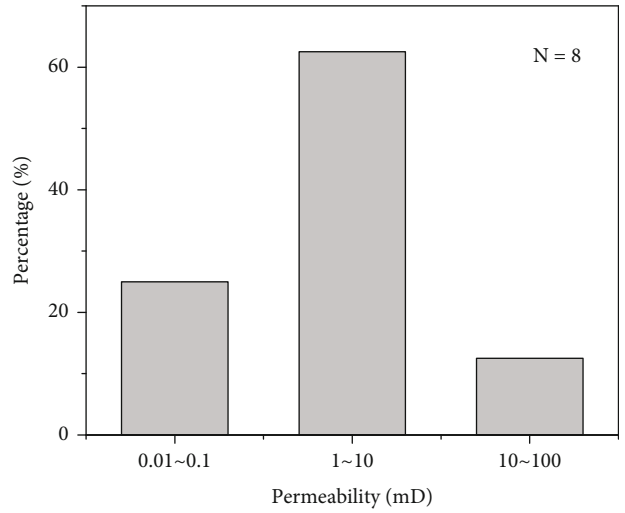

Figure 12: Permeability distribution histogram with microfractures.

in this section was low, and a large number of organisms formed colonies here for an extended period of time, resulting in bioturbation

4.5. Shale Water Cut Characteristics. NMR experimental tests were run on 18 samples of Longmaxi Formation shale from wells L1 and L2. The integral area of the T2 distribution curve represents the amount of fluid content in the rock pores (Figure 16). The results show that the movable fluid saturation of eight samples from well L1 ranged from 3.32% to 67.57%, with an average of 19.72%, and bound water saturation ranged from 32.43% to 96.68%, with an average of 80.23%. The movable fluid saturation in 10 samples from well L2 ranged from 33.25% to 66.73%, with an average of 46.95%, while the bound water saturation ranged from 33.27% to 66.73%, with an average of 53.05%.

Table 3: Pore structure parameters in the study area.

Sample number	Depth (m)	BET-specific surface area (m^2/g)	BJH Vtotal (cm^3/g)	Mean pore diameter (nm)
L1-1	1027.00	17.50	0.0265	8.60
L1-7	1039.45	16.20	0.0248	8.40
L1-14	1057.97	23.00	0.0331	8.40
L1-17	1063.05	23.30	0.0332	8.40
L2-1	1654.40	19.30	0.0316	10.00
L2-3	1659.96	20.80	0.0327	9.70
L2-5	1665.68	21.00	0.0326	9.90
L2-7	1668.77	22.10	0.0340	9.70
L3-3	1479.25	23.34	0.0328	8.98
L3-5	1483.29	22.20	0.0314	9.10
L3-8	1489.52	26.26	0.0344	8.67
L3-11	1498.56	27.13	0.0340	8.34

Table 5 shows that the movable fluid saturation value of well L1 is low, while the saturation of irreducible water is high and contains a large amount of water, which proves that the permeability of well L1 is poor. Compared to well L1, well L2 has a higher saturation value of movable fluid, a lower irreducible water saturation, less water cut, and predictably better permeability.

5. Discussion

5.1. The Effect of Organic Matter on Permeability. Previous observations by scanning electron microscopy have shown that organic pores have better connectivity than other inter- and intraparticle pores [40]. Therefore, organic pores are the main pore system for natural gas flow in shale [40, 41]. By observing the relationship between organic matter characteristics and vertical permeability of the overburden (Figure 17), we conclude that vertical permeability has a weak positive correlation with TOC. In the process of hydrocarbon generation, condensation of organic matter and volume expansion during gas generation results in the formation of a large number of pores in organic matter [3, 42]. Organic matter content in shale is a significant controlling factor for the development of organic pores. The enrichment and formation of nanoscale pores within organic matter particles is associated with the maturation of organic matter into hydrocarbons, mainly due to bubble generation from liquid or gas accumulation [3]. Furthermore, diagenesis leads to organic matter debris dehydrogenation and angiogenesis as it matures, causing an increase in organic matter content in pores [43]. In general, the characteristics of organic matter have a certain impact on the vertical permeability of shale, since organic matter pores account for a large proportion of shale rocks, while other types of pores are less prevalent. A higher organic matter content is correlated to a higher maturity of the organic matter, which proves that an increase in organic pores leads to an increase of vertical permeability in shale.

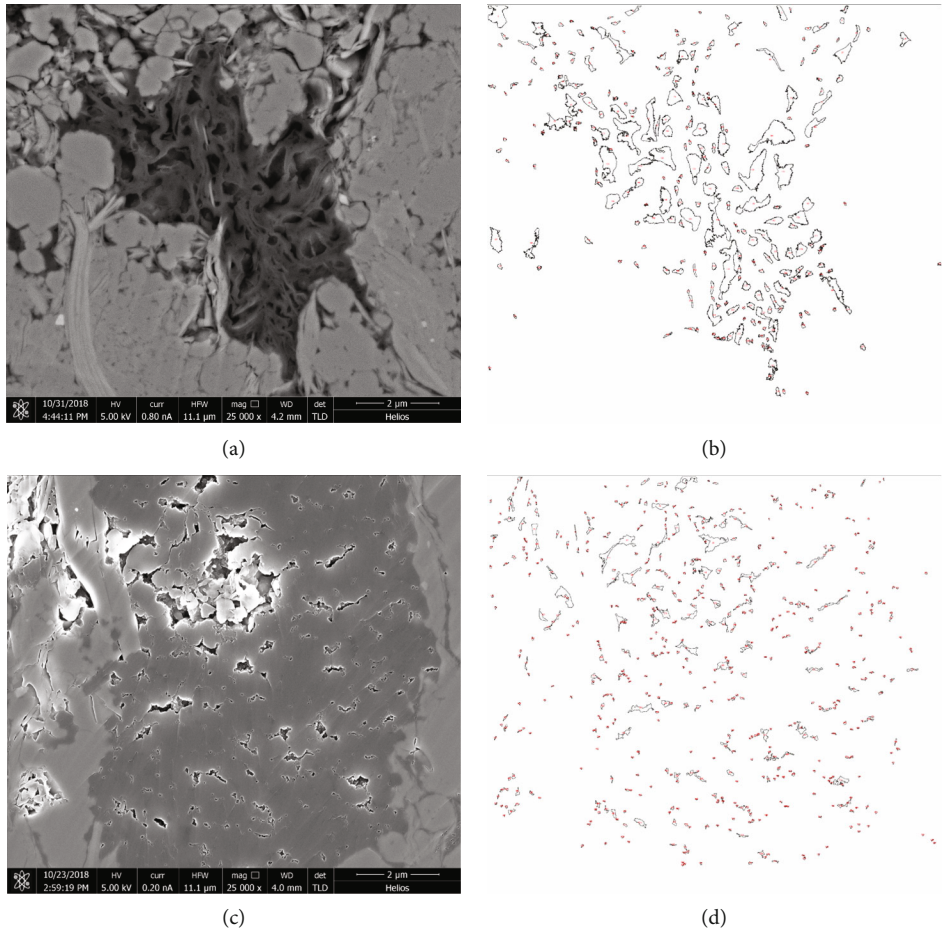

Figure 13: SEM pore extraction from shale samples. (a) L1-14 original SEM image. (b) L1-14 SEM pore extraction. (c) L1-20 original SEM image. (d) L1-20 SEM pore extraction.

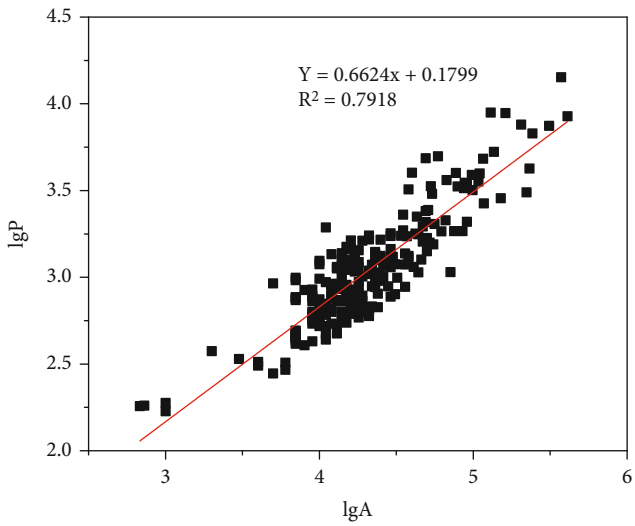

Figure 14: Fractal characteristics of pore morphology in shale SEM.

5.2. Influence of Lithofacies and Minerals on Permeability

5.2.1. Influence of Mineral Fraction on Permeability. In the samples studied, there is a negative relevance between TOC and permeability, indicating that other factors may also have an impact on permeability. Quartz content in well L1 is positively correlated with permeability (Figure 18(a)) and shows a weak negative correlation with both carbonate and clay mineral contents (Figures 18(b) and 18(c)). The positive correlation between TOC and quartz content suggests a biological origin for quartz in the study area (Figure 19(a)). First, the increase in the content of quartz means that an increase in the number of organic pores, followed by an abundance of quartz that protects the primary pores from destruction, results in increased permeability [22, 44]. Carbonate rock has a complex effect on permeability. On the one hand, carbonate can block micropores and mesoporous pores. On the other hand, the dissolution of carbonate leads to the development of erosive pores and the enhancement of pore connectivity [26]. Carbonate minerals may have blocked the pores in the sample from well L1. Quartz and clay in wells L2 and L3 have a weak negative correlation with permeability (Figures 18(a) and 18(c)). It is indicated that the permeability rate did not increase as the content of

Table 4: Shale SEM pore extraction results.

Sample number	NMR porosity (%)	Porosity (%)	Interstitial surface area (nm^2)	Perimeter (nm)	Roundness	Fractal dimension
L1-14	6.64	7.10	504.00~1365000.00 (21749.98)	103.00~17294.00 (807.04)	0.002~1.000 (0.506)	0.58
L1-20	6.09	1.93	160.20~485000.00 (6095.55)	51.00~10593.00 (359.44)	0.025~0.991 (0.454)	0.66
L1-26	5.95	1.94	636.30~410000.00 (9719.11)	98.00~14224.00 (551.94)	0.044~0.967 (0.469)	0.59

(a) (b)

(c) (d)

(c) (d)

(e) (f)

(e) (f)

Figure 15: Characteristics of Longmaxi Formation shale in the study area. (a) Gray-black shale, horizontal bedding, well L1, 1026.35 m. (b) Gray-black shale, horizontal bedding, well L1, 1037.19 m. (c) Black shale, massive bedding, well L1, 1055.42 m. (d) Black shale, massive bedding, vertical fractures developed, well L1, 1061.25 m. (e) Black shale, massive bedding, well L1, 1062.62 m. (f) Black shale, massive bedding and horizontal bedding, well L1, 1073.81 m.

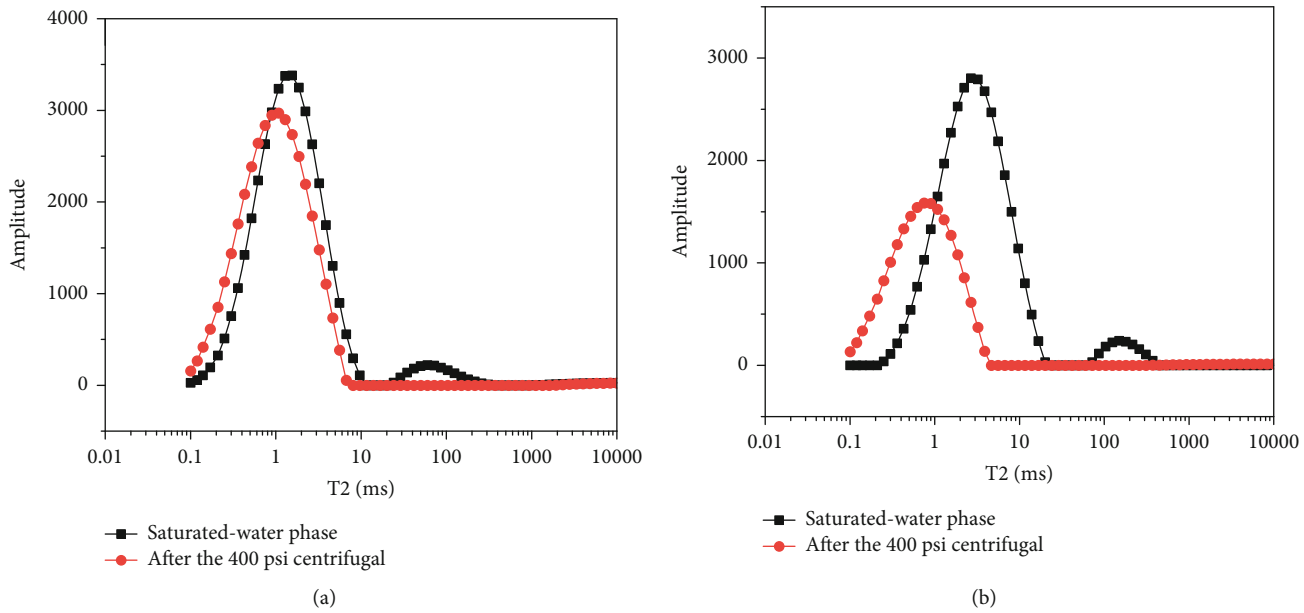

Figure 16: NMR T2 spectrum. (a) L1-20 NMR T2 spectrum. (b) L1-26 NMR T2 spectrum.

Table 5: NMR movable fluid saturation results.

Sample number	Porosity (%)	Overburden vertical permeability (mD)	K/Φ	Movable fluid saturation (%)	Irreducible water saturation (%)
L1-20	6.09	0.00017	0.0010353	3.32	96.68
L1-26	5.95	0.00087	0.0051765	45.04	54.96
L2-1	5.9	0.00097	0.005723	66.73	33.27
L2-3	5.07	0.00066	0.0033462	38.86	61.14
L2-5	7.76	0.00111	0.0086136	46.89	53.11
L2-14	6.99	0.00061	0.0042639	45.68	54.32

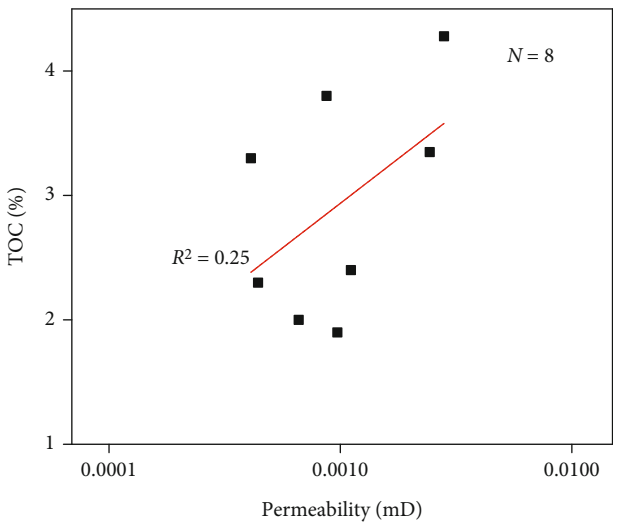

Figure 17: Relationship between overburden vertical permeability and TOC.

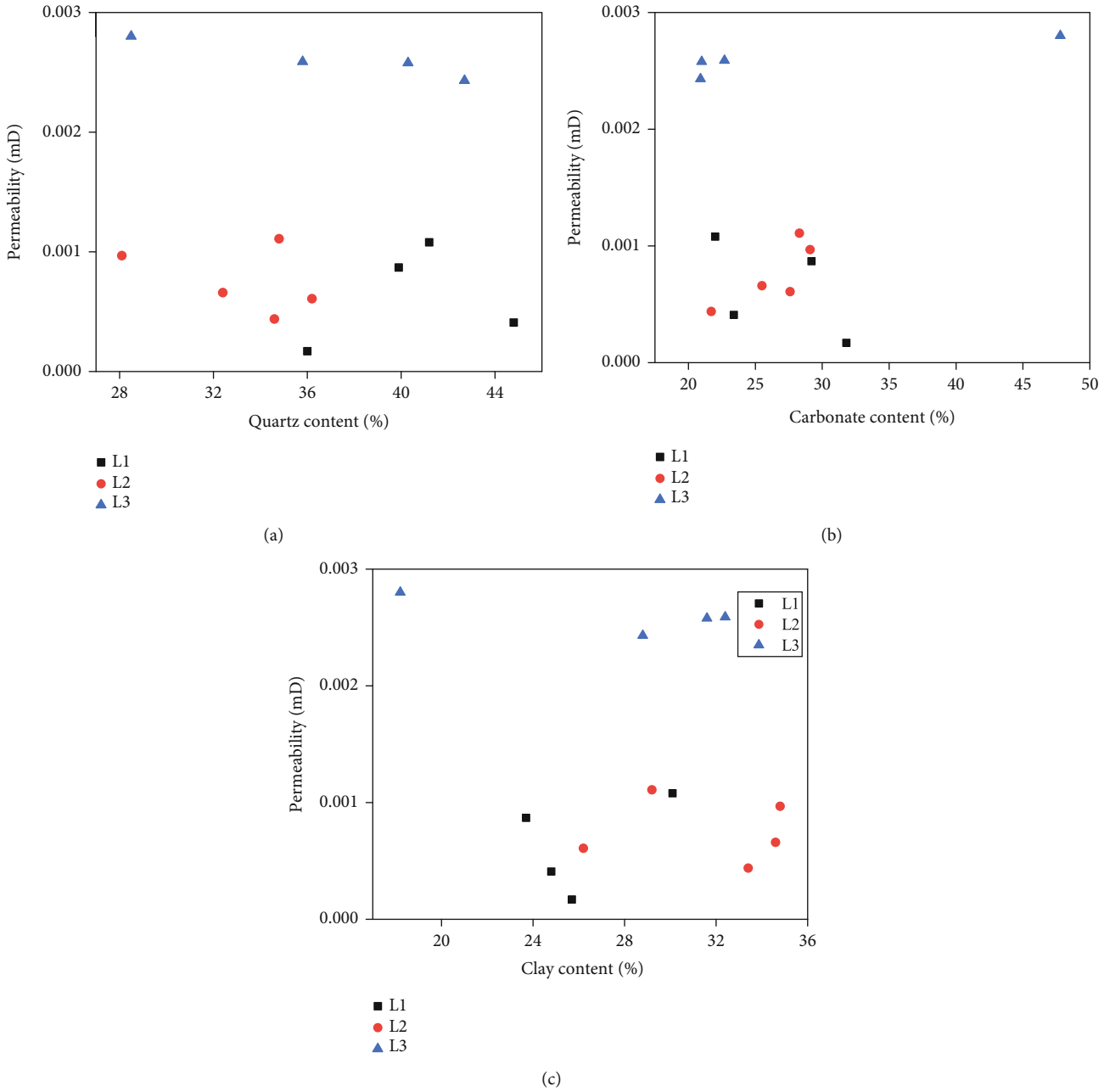

Figure 18: Relationship between shale mineral composition and permeability. (a) Permeability vs. quartz content. (b) Permeability vs. carbonate content. (c) Permeability vs. clay content.

quartz and clay increased, although the pores between the grains increased. In the TOC-mineral relationship (Figure 19(b)), TOC shows a strong negative correlation with clay minerals, indicating that as clay minerals increase, organic matter decreases, and organic pores decrease. It is also possible that clay minerals block the pores and form pores that are not well connected, thus showing a negative correlation. However, in the pores of wells L2 and L3, carbonate has a certain positive effect on permeability, which proves that the dissolution of carbonate causes the increase of pore connectivity.

5.2.2. The Effect of Lithofacies on Permeability. By identifying each shale facies and considering the permeability differences between lithofacies (Figure 20), we conclude that the lithofacies with the best permeability of the studied shales is the siliceous clay mixed shale facies. On the other hand, the lithofacies with the worst permeability is the mixed shale facies.

(1) Mixed shale facies and shale permeability: it is evident that the permeability of the mixed shale phase is lower than the other two shale phases despite

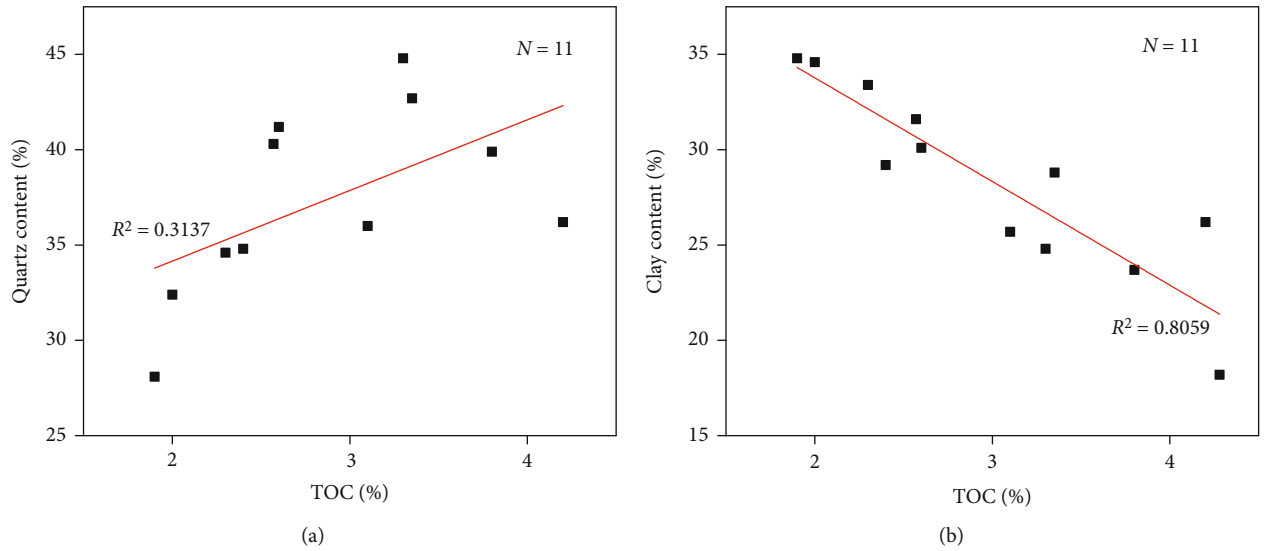

Figure 19: Relationship between organic carbon and mineral content. (a) Quartz content vs. TOC. (b) Clay content vs. TOC.

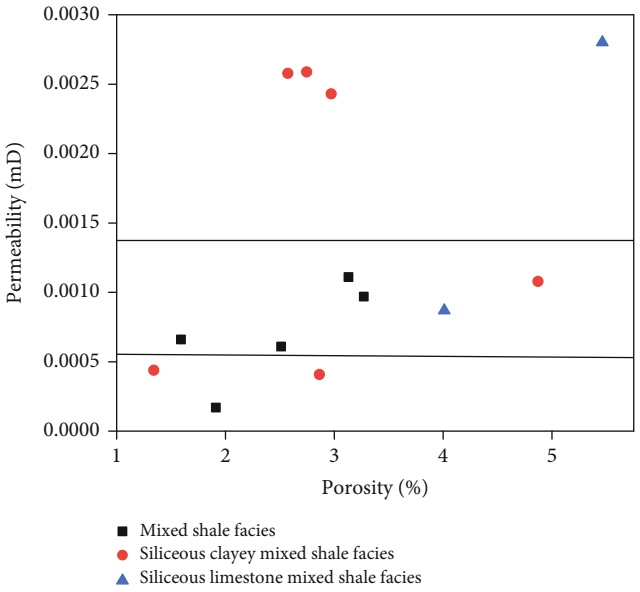

Figure 20: Permeability of different lithofacies.

having similar porosity characteristics. The phase was formed in an anoxic reducing environment, and its components do not differ greatly in content, so it is possible that the latter interacted with each other, resulting in low permeability

(2) Siliceous clay mixed shale facies and shale permeability: the higher silica content may favor the preservation of pore spaces and howler channels, resulting in better permeability of this facies. Some of phases present in these facies are less permeable, possibly due to clay minerals blocking pore throats and thus reducing permeability

(3) Siliceous-calcareous mixed shale facies and shale permeability: compared to the siliceous shale phase, the siliceous-calcite-bearing mixed shale phase contains a certain amount of calcium, which is presumed to have a slightly deeper sedimentary water column and a slightly stronger sedimentary hydrodynamic environment than the siliceous shale phase, thus leading to a greater difference in permeability between the two samples

5.3. Influence of Pore Characteristics on Permeability. Based on the results obtained for pore structure parameters in shales of the Longmaxi Formation, there appears to be a relationship between shale permeability and pore structure in the studied samples. Organic pores in shale lead to a higher BET-specific surface area, and higher pore content in shale is reflected in a higher total pore volume. In addition, the relationship between BET surface area, BJH total pore volume, and permeability indicates that as BET-specific surface area and BJH total pore volume increase, the permeability of shale increases (Figures 21(a) and 21(b)). Conversely, a weak negative relevance between pore size and permeability can be seen in the relationship between pore size and permeability (Figure 21(c)), indicating that larger pores are more likely to be plugged by infill clastic minerals. The pore fractal dimension shows a negative correlation with permeability (Figure 21(d)); the simpler the pore structure of the shale, the higher the permeability of the sample will be.

5.4. The Effect of Bedding on Permeability. Bedding is the main factor that causes anisotropy in permeability, and the permeability measured along horizontal bedding in this study (Figure 22) is much higher than that measured along vertical bedding. In shale, due to the existence of a lamellar structure in clay minerals, mineral particles and pores are

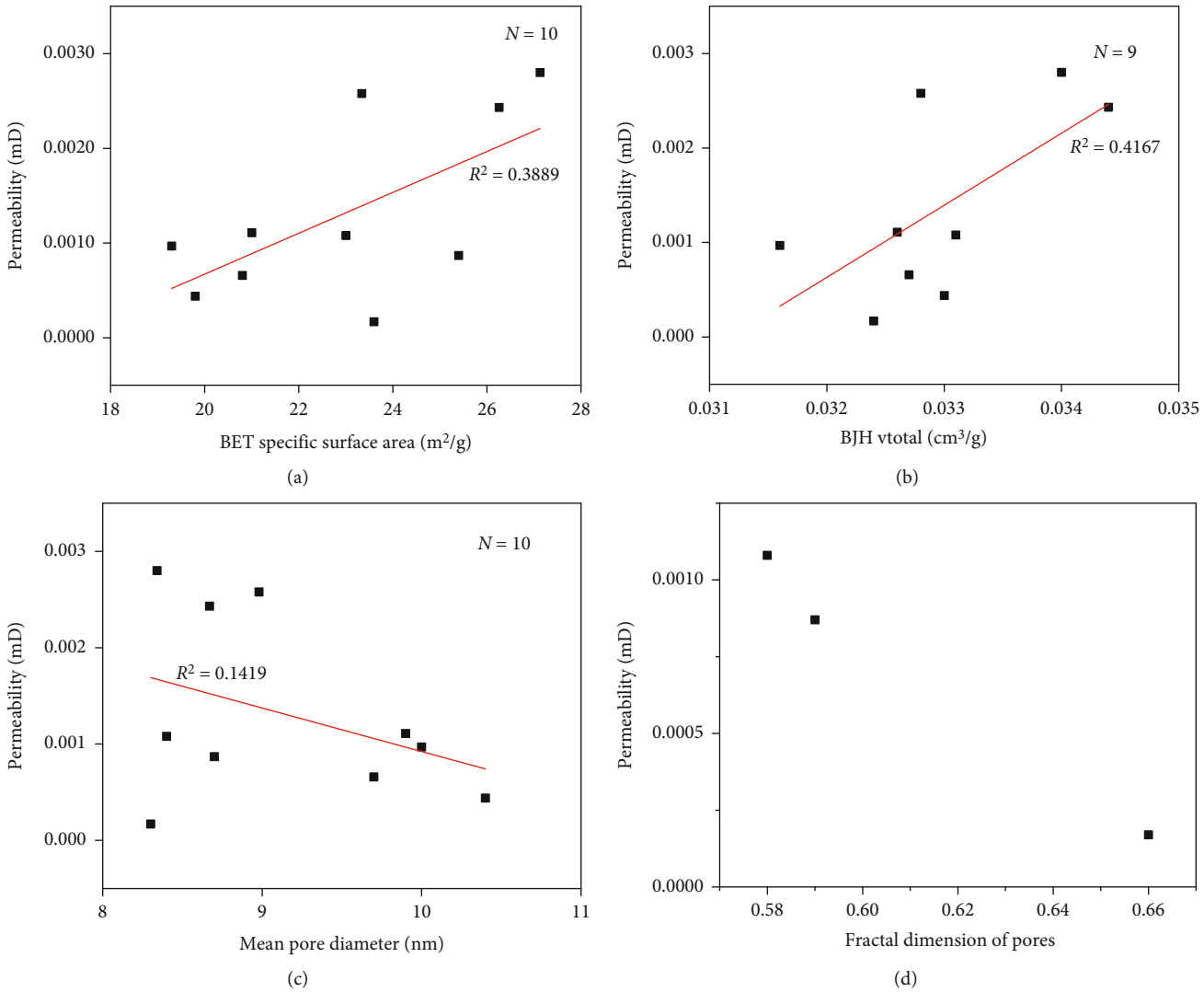

Figure 21: Pore structure parameters and permeability. (a) Permeability vs. BET-specific surface area. (b) Permeability vs. BJH Vtotal. (c) Permeability vs. mean pore diameter. (d) Permeability vs. pore fractal dimension.

often arranged in layers [38]. Since bedding is the manifestation of changes in mineral composition, bedding is a weak contact surface of the rock [45], and seepage channels will appear between laminae of different grain sizes. Thus, pore connectivity along horizontal bedding is better than along vertical layers. In addition, microcracks often follow the bedding directions. Therefore, bedding plays a pivotal role in the anisotropy of permeability.

5.5. The Effect of Water Content on Permeability. Organic kerogen is hydrophobic, and water has little influence on organic pores. However, shale gas migration in inorganic pores is significantly affected by water. In addition, the influence of clay mineral content on the occurrence of movable fluid is mainly exerted by the joint effect of various clay minerals, since the influence of a single clay mineral is relatively limited [46]. It is worth noting that the presence of clay minerals in shale is the main factor for water retention in reservoirs [47]. Irreducible water saturation in the study area increases with the rise of the content of the illite/smectite (I/S) mixed layer, which indicates that the I/S mixed layer will absorb water, resulting in water retention in the shale (Figure 23). According to the cross-plot of irreducible water saturation and permeability (Figure 24), higher contents of comfortable water correlate with decreased permeability. The reasons why water content affects the permeability of shale include the following: (1) as the shale mixed layer absorbs large amounts of water, clay minerals will expand, block pores or cracks, and penetrate into microfractures and matrix pores. As a result, permeability is greatly reduced (Figure 22). (2) Stagnant water will block the flow channel, leading to decreased seepage capacity of fractures and affecting pore connectivity [48, 49]. The permeability vs. porosity ratio (K/Φ) is closely related to the composition of rock particles, pore connectivity, pore geometry, and particle compaction, among other parameters. This ratio

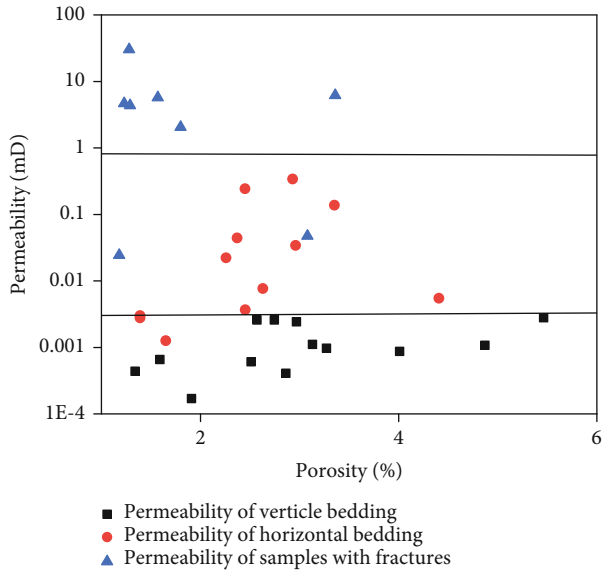

Figure 22: Distribution of different types of porosity and permeability under overburden pressure test.

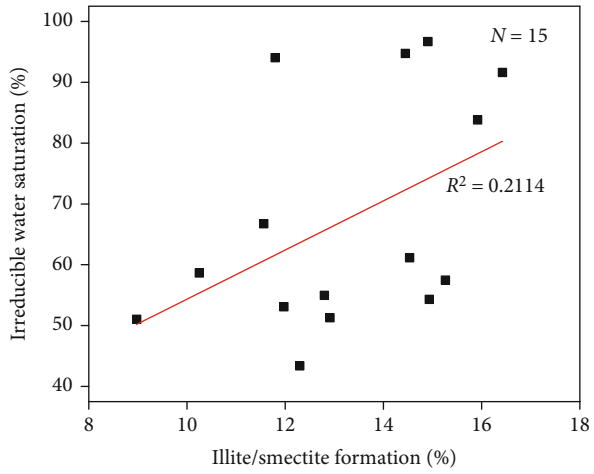

Figure 23: Irreducible water saturation vs. illite/smectite formation.

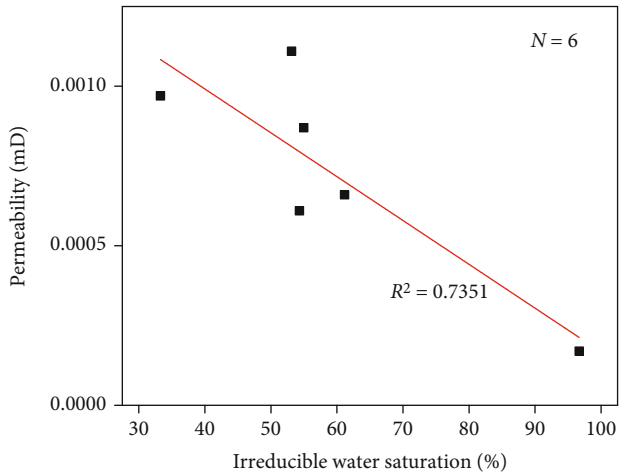

Figure 24: Permeability vs. irreducible water saturation.

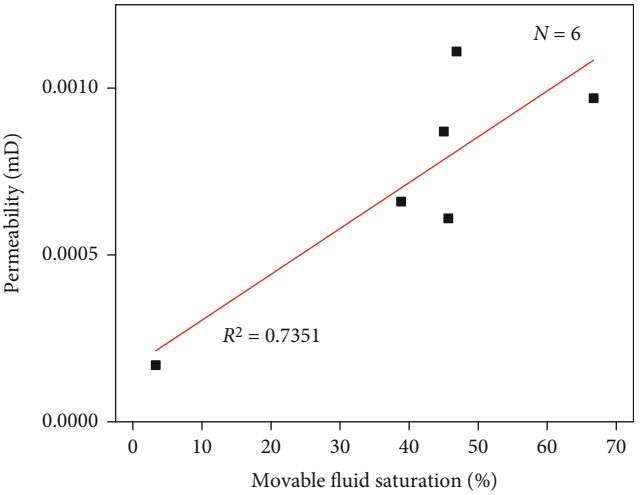

Figure 25: Movable fluid saturation and permeability.

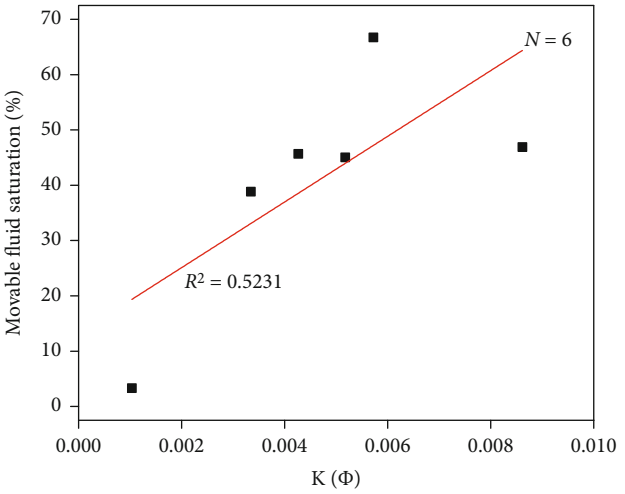

Figure 26: Correlation between movable fluid and K/Φ.

comprehensively reflects the relationship between the basic physical properties of the rock and movable fluid saturation, which reflects the quality of the reservoir rock, and reflects the seepage ability of the reservoir rock [50–54]. As depicted in Figures 25 and 26, movable fluid saturation correlates positively with the permeability of the lithology.

6. Conclusions

(1) Shale in the study area corresponds to overmature organic-rich shale. Since the abundance and maturity of organic matter control the development of organic pores and the permeability of organic pores in these samples is relatively good, high TOC and high maturity improve the permeability of these shales

(2) Shale bedding in the study area is the key controlling factor for the anisotropy of shale permeability.

Mineral composition and rock relative permeability also influence permeability to some extent, since different minerals have different effects on shale permeability. Clay can expand and produce cracks to improve permeability; however, it can also block pore throats and reduce permeability. In the study area, clay has an adverse effect on permeability. The effect of quartz and carbonate minerals on permeability is also twofold. In the study area, the organic-rich siliceous clay mixed shale has the highest permeability. Pore structure characteristics also have an impact on permeability. A larger specific surface area and total pore volume lead to increased permeability of shale, while average pore size has no correlation with permeability. A smaller fractal dimension of pore shapes and a simpler pore structure also lead to better permeability

(3) Water in shale can affect the permeability of microfractures by combining with clay minerals. The permeability of shale with high bound water saturation is low, indicating that water and clay minerals absorbing water may block flow channels and lead to poor permeability

Data Availability

The experimental data used to support the findings of this study are included within the manuscript and the supplementary materials (available here).

Conflicts of Interest

The authors declare that there are no conflicts of interest regarding the publication of this paper.

Acknowledgments

The authors would like to extend their gratitude to the Natural Science Foundation of Xinjiang Uygur Autonomous Region (Grant No. 2020D01C037), the National Natural Science Foundation of China (Grant No. 42062010), the Tianshan Innovation Team Program (2020D14023), and the Innovation Program for College Students (S202110755003).

Supplementary Materials

Geochemical analysis: organic geochemical analyses include total organic matter content, organic matter maturity, and cheese root type. Organic matter content tests allow analysis of the reservoir's hydrocarbon potential and organic matter pore development to evaluate the effect on permeability. Specific surface area and pore size measurements: specific surface area and pore measurements include BET-specific surface area and BJH total pore volume and average pore diameter, which are measured to investigate their relationship with permeability. NMR experiment: NMR experiment can be used to obtain the fluid saturation and bound water saturation in pores, and the relationship between water saturation and permeability can be studied by this test. XRD whole rock analysis: XRD analysis gives the content of most minerals, and this study is used to determine the effect of mineral composition on permeability. *(Supplementary Materials)*

References

[1] J. B. Curtis, "Fractured shale-gas systems," *AAPG Bulletin*, vol. 86, no. 11, pp. 1921–1938, 2002.

[2] M. N. Ge, F. Pang, and S. J. Bao, "Micro pore characteristics of Wufeng-Longmaxi shale and their control on gas content: a case study of well Anye 1 in Zunyi area, Guizhou province," *Petroleum Geology & Experiment*, vol. 41, no. 01, pp. 23–30, 2019.

[3] D. M. Jarvie, R. J. Hill, T. E. Ruble, and R. M. Pollastro, "Unconventional shale-gas systems: the Mississippian Barnett shale of North-Central Texas as one model for thermogenic shale-gas assessment," *AAPG Bulletin*, vol. 91, no. 4, pp. 475–499, 2007.

[4] J. Li, X. B. Wang, L. H. Hou et al., "Geochemical characteristics and resource potential of shale gas in Sichuan basin, China," *Journal of Natural Gas Geoscience*, vol. 6, no. 6, pp. 313–327, 2021.

[5] J. C. Zhang, Z. J. Jin, and M. S. Yuan, "Reservoiring mechanism of shale gas and its distribution," *Natural Gas Industry*, vol. 24, no. 7, pp. 15–18, 2004.

[6] C. N. Zou, D. Z. Dong, S. J. Wang et al., "Geological characteristics and resource potential of shale gas in China," *Petroleum Exploration and Development*, vol. 37, no. 6, pp. 641–653, 2010.

[7] M. E. Curtis, B. J. Cardott, C. H. Sondergeld, and C. S. Rai, "Development of organic porosity in the Woodford shale with increasing thermal maturity," *International Journal of Coal Geology*, vol. 103, pp. 26–31, 2012.

[8] O. Iqbal, E. Padmanabhan, A. Mandal, and J. Dvorkin, "Characterization of geochemical properties and factors controlling the pore structure development of shale gas reservoirs," *Journal of Petroleum Science and Engineering*, vol. 206, p. 109001, 2021.

[9] C. Z. Jia, "Breakthrough and significance of unconventional oil and gas to classical petroleum geology theory," *Petroleum Exploration and Development*, vol. 44, no. 1, pp. 1–10, 2017.

[10] S. A. Solarin, L. A. Gil-Alana, and C. Lafuente, "An investigation of long range reliance on shale oil and shale gas production in the U.S. market," *Energy*, vol. 195, p. 116933, 2020.

[11] R. Weijermars, N. Sorek, D. Sen, and W. B. Ayers, "Eagle ford shale play economics: U.S. versus Mexico," *Journal of Natural Gas Science and Engineering*, vol. 38, pp. 345–372, 2017.

[12] C. N. Zou, Q. Zhao, G. S. Zhang, and B. Xiong, "Energy revolution: from a fossil energy era to a new energy era," *Natural Gas Industry*, vol. 3, no. 1, pp. 1–11, 2016.

[13] H. Wang, Z. H. Kou, D. A. Bagdonas et al., "Multiscale petrophysical characterization and flow unit classification of the Minnelusa Eolian sandstones," *Journal of Hydrology*, vol. 607, p. 127466, 2022.

[14] C. N. Zou, Z. Yang, G. S. ZHang et al., "Establishment and practice of unconventional oil and gas geology," *Acta Geologica Sinica*, vol. 93, no. 01, pp. 12–23, 2019.

[15] Z. J. Jin, Z. Q. Hu, B. Gao, and J. H. Zhao, "Controlling factors on the enrichment and high productivity of shale gas in the Wufeng-Longmaxi formations, southeastern Sichuan basin," *Earth Science Frontiers*, vol. 23, no. 1, pp. 1–10, 2016.

[16] D. Z. Dong, S. K. Gao, J. L. Huang, Q. Z. Guan, S. F. Wang, and Y. M. Wang, "A discussion on the shale gas exploration & development prospect in the Sichuan basin," *Natural Gas Industry*, vol. 34, no. 12, pp. 1–15, 2015.

[17] D. Dong, Z. Shi, Q. Guan et al., "Progress, challenges and prospects of shale gas exploration in the Wufeng-Longmaxi reservoirs in the Sichuan basin," *Natural Gas Industry*, vol. 38, no. 4, pp. 67–76, 2018.

[18] X. H. Ma and J. Xie, "The progress and prospects of shale gas exploration and development in southern Sichuan basin, SW China," *Petroleum Exploration and Development*, vol. 45, no. 1, pp. 172–182, 2018.

[19] G. Y. Zhai, Y. F. Wang, S. J. Bao et al., "Major factors controlling the accumulation and high productivity of marine shale gas and prospect forecast in southern China," *Earth Science*, vol. 42, no. 7, pp. 1057–1068, 2017.

[20] H. Y. Qu, Z. J. Pan, Y. Peng, and F. J. Zhou, "Controls on matrix permeability of shale samples from Longmaxi and Niutitang formations, China," *Journal of Natural Gas Science and Engineering*, vol. 33, pp. 599–610, 2016.

[21] W. Zhang and Q. Wang, "Permeability anisotropy and gas slippage of shales from the Sichuan basin in South China," *International Journal of Coal Geology*, vol. 194, pp. 22–32, 2018.

[22] G. R. L. Chalmers, D. J. K. Ross, and R. M. Bustin, "Geological controls on matrix permeability of Devonian gas shales in the Horn River and Liard basins, northeastern British Columbia, Canada," *International Journal of Coal Geology*, vol. 103, pp. 120–131, 2012.

[23] D. Davudov, R. G. Moghanloo, and Y. X. Zhang, "Interplay between pore connectivity and permeability in shale sample," *International Journal of Coal Geology*, vol. 220, p. 103427, 2020.

[24] O. Kwon, A. K. Kronenberg, A. F. Gangi, B. Johnson, and B. E. Herbert, "Permeability of illite-bearing shale: 1. Anisotropy and effects of clay content and loading," *Journal of Geophysical Research: Solid Earth*, vol. 109, no. B10, 2004.

[25] G. G. Lash and T. Engelder, "An analysis of horizontal microcracking during catagenesis: example from the Catskill delta complex," *AAPG Bulletin*, vol. 89, no. 11, pp. 1433–1449, 2005.

[26] Q. T. Wang, T. L. Wang, W. P. Liu et al., "Relationships among composition, porosity and permeability of Longmaxi shale reservoir in the Weiyuan block, Sichuan basin, China," *Marine and Petroleum Geology*, vol. 102, pp. 33–47, 2019.

[27] Q. Lyu, J. D. Shi, J. Q. Tan, J. M. Dick, and X. Kang, "Effects of shale swelling and water-blocking on shale permeability," *Journal of Petroleum Science and Engineering*, vol. 212, p. 110276, 2022.

[28] M. M. Meng, H. K. Ge, Y. H. Shen, L. L. Li, T. H. Tian, and J. Chao, "The effect of clay-swelling induced cracks on shale permeability during liquid imbibition and diffusion," *Journal of Natural Gas Science and Engineering*, vol. 83, no. 2, p. 103514, 2020.

[29] X. P. Zhou and Z. Zhao, "Digital evaluation of nanoscale-pore shale fractal dimension with microstructural insights into shale permeability," *Journal of Natural Gas Science and Engineering*, vol. 75, p. 103137, 2020.

[30] Y. L. Tan, S. H. Zhang, S. H. Tang et al., "Impact of water saturation on gas permeability in shale: experimental and modelling," *Journal of Natural Gas Science and Engineering*, vol. 95, no. 3, p. 104062, 2021.

[31] Y. S. Pan, Z. L. Huang, X. B. Guo, B. C. Liu, G. Q. Wang, and X. F. Xu, "Study on the pore structure, fluid mobility, and oiliness of the lacustrine organic-rich shale affected by volcanic ash from the Permian Lucaogou formation in the Santanghu basin, Northwest China," *Journal of Petroleum Science and Engineering*, vol. 208, no. 3, p. 109351, 2022.

[32] Z. Y. Wang, L. Chen, D. X. Chen et al., "Characterization and evaluation of shale lithofacies within the lowermost Longmaxi-Wufeng formation in the Southeast Sichuan basin," *Journal of Petroleum Science and Engineering*, vol. 193, p. 107353, 2020.

[33] C. Yang, J. C. Zhang, and X. Tang, "Microscopic pore types and its impact on the storage and permeability of continental shale gas, Ordos Basin," *Earth Science Frontiers*, vol. 20, no. 04, pp. 240–250, 2013.

[34] W. M. Ji, Y. Song, Z. X. Jiang et al., "Micro-nano pore structure characteristics and its control factors of shale in Longmaxi formation, southeastern Sichuan basin," *Acta Petrolei Sinica*, vol. 37, no. 2, pp. 182–195, 2016.

[35] P. F. Zhang, S. F. Lu, J. Q. Li, H. T. Xue, W. B. Li, and S. Y. Wang, "Quantitative characterization of microscopic pore structure for shales using scanning electron microscopy," *Journal of China University of Petroleum (Edition of Natural Science)*, vol. 42, no. 2, pp. 19–28, 2018.

[36] D. Z. Dong, Z. S. Shi, S. S. Sun et al., "Factors controlling microfractures in black shale: a case study of Ordovician Wufeng formation–Silurian Longmaxi formation in Shuanghe profile, Changning area, Sichuan basin, SW China," *Petroleum Exploration and Development*, vol. 45, no. 5, pp. 818–829, 2018.

[37] Z. S. Shi, D. Z. Dong, H. Y. Wang, S. S. Sun, and J. Wu, "Reservoir characteristics and genetic mechanisms of gas-bearing shales with different laminae and laminae combinations: a case study of member 1 of the lower Silurian Longmaxi shale in Sichuan basin, SW China," *Petroleum Exploration and Development*, vol. 47, no. 4, pp. 888–900, 2020.

[38] Z. S. Shi and Z. Qiu, "Main bedding types of marine fine-grained sediments and their significance for oil and gas exploration and development," *Acta Sedimentologica Sinica*, vol. 39, no. 1, pp. 181–196, 2021.

[39] Z. S. Shi, Z. Qiu, D. Z. Dong, B. Lu, P. P. Liang, and M. Q. Zhang, "Lamina characteristics of gas-bearing shale fine-grained sediment of the Silurian Longmaxi formation of well Wuxi 2 in Sichuan basin, SW China," *Petroleum Exploration and Development*, vol. 45, no. 2, pp. 358–368, 2018.

[40] R. G. Loucks, R. M. Reed, S. C. Ruppel, and U. Hammes, "Spectrum of pore types and networks in mudrocks and a descriptive classification for matrix-related mudrock pores," *AAPG Bulletin*, vol. 96, no. 6, pp. 1071–1098, 2012.

[41] R. J. Ambrose, R. C. Hartman, and Y. Akkutlu, "New pore-scale considerations for shale gas in place calculations," in *SPE unconventional gas conference*, Pittsburgh, Pennsylvania, USA, February 2010.

[42] C. J. Modica and S. G. Lapierre, "Estimation of kerogen porosity in source rocks as a function of thermal transformation: example from the Mowry shale in the Powder River basin of Wyoming," *AAPG Bulletin*, vol. 96, no. 1, pp. 87–108, 2012.

[43] L. Huang and W. Shen, "Characteristics and controlling factors of the formation of pores of a shale gas reservoir: a case study from Longmaxi formation of the Upper Yangtze region, China," *Earth Science Frontiers*, vol. 22, no. 1, pp. 374–385, 2015.

[44] T. Dong, N. B. Harris, K. Ayranci, C. E. Twemlow, and B. R. Nassichuk, "The impact of composition on pore throat size and permeability in high maturity shales: middle and upper Devonian Horn River group, northeastern British Columbia, Canada," *Marine and Petroleum Geology*, vol. 81, pp. 220–236, 2017.

[45] W. Y. Zhu and D. X. Ma, "Effect of bedding seam on shale permeability and its characterization," *Special Oil & Gas Reservoirs*, vol. 25, no. 02, pp. 130–133, 2018.

[46] N. Zhang, Z. Y. Zhang, and S. D. Wang, "A review on calculation of movable fluid saturation of low permeability oil reservoir and its influencing factors water," *Resources and Hydropower Engineering*, vol. 52, no. 09, pp. 143–155, 2021.

[47] H. J. Mao, Y. T. Guo, G. J. Wang, and C. H. Yang, "Evaluation of impact of clay mineral fabrics on hydration process," *Rock and Soil Mechanics*, vol. 31, no. 9, pp. 2723–2728, 2010.

[48] L. J. You, B. B. Xie, J. Yang et al., "Mechanism of fracture damage induced by fracturing fluid flowback in shale gas reservoirs," *Natural Gas Industry*, vol. 38, no. 12, pp. 61–69, 2018.

[49] W. Y. Zhu, B. C. Wang, D. X. Ma, K. Huang, and B. B. Li, "Effect of water on seepage capacity of shale with microcracks," *Natural Gas Geoscience*, vol. 31, no. 3, pp. 317–324, 2020.

[50] H. K. Wu, K. Cao, and F. F. Zhao, "NMR experimental study of movable fluid saturation in low permeability sedimentary rocks," *Natural Gas Geoscience*, vol. 32, no. 03, pp. 457–463, 2021.

[51] H. Deng, G. L. Sheng, H. Zhao et al., "Integrated optimization of fracture parameters for subdivision cutting fractured horizontal wells in shale oil reservoirs," *Journal of Petroleum Science and Engineering*, vol. 212, p. 110205, 2022.

[52] G. L. Sheng, Y. L. Su, and W. D. Wang, "A new fractal approach for describing induced-fracture porosity/permeability/ compressibility in stimulated unconventional reservoirs," *Journal of Petroleum Science and Engineering*, vol. 179, pp. 855–866, 2019.

[53] G. D. Cui, T. Liu, J. Y. Xie, G. H. Rong, and L. H. Yang, "A review of SAGD technology development and its possible application potential on thin-layer super-heavy oil reservoirs," *Geoscience Frontiers*, vol. 13, no. 4, p. 101382, 2022.

[54] G. D. Cui, F. L. Ning, B. Dou, T. Li, and Q. C. Zhou, "Particle migration and formation damage during geothermal exploitation from weakly consolidated sandstone reservoirs via water and CO_2 recycling," *Energy*, vol. 240, p. 122507, 2022.